

REAL-TIME SIMULATION OF THE GOES-R ABI FOR USER READINESS AND PRODUCT EVALUATION

BY THOMAS J. GREENWALD, R. BRADLEY PIERCE, TODD SCHAACK, JASON OTKIN, MAREK ROGAL, KABA BAH, ALLEN LENZEN, JIM NELSON, JUN LI, AND HUNG-LUNG HUANG

Simulated Advanced Baseline Imager (ABI) data are vital for evaluating product algorithms, testing data systems, and preparing users for the next generation of Geostationary Operational Environmental Satellite (GOES) data.

The decade-long preparation for the launch of the Geostationary Operational Environmental Satellite R series (GOES-R) slated for late 2016 represents a major effort involving hundreds of scientists and engineers from government agencies,

private companies, and universities. Three main activities were established within the GOES-R program to ensure that reliable, high quality data products are available from the Advanced Baseline Imager (ABI), Geostationary Lightning Mapper, and space environment instruments once the GOES-R is launched and that users will be well prepared to use these new products.

The first of these, with an emphasis on making use of data from multiple sources [e.g., satellite, radar, numerical weather prediction (NWP) models, surface observations], is the GOES-R Risk Reduction (GOES-R3) program, which promotes advanced applications that directly benefit operational forecasters. The GOES-R3 program supports a broad range of research for the ABI, from data assimilation, ocean currents, land surface properties, and atmospheric composition to severe weather, visibility hazards, flash floods, and aircraft icing. Participants include the Cooperative Institute for Climate and Satellites (CICS) at the University of Maryland, the Cooperative Institute for Meteorological Satellite Studies (CIMSS) at the University of Wisconsin–Madison, the

AFFILIATIONS: GREENWALD, SCHAACK, OTKIN, ROGAL, BAH, LENZEN, NELSON, LI, AND HUANG—Cooperative Institute for Meteorological Satellite Studies, University of Wisconsin–Madison, Madison, Wisconsin; PIERCE—NOAA/National Environmental Satellite, Data, and Information Service, Madison, Wisconsin

CORRESPONDING AUTHOR: Thomas J. Greenwald, Cooperative Institute for Meteorological Satellite Studies, University of Wisconsin–Madison, 1225 West Dayton St., Madison, WI 53706
E-mail: tomg@ssec.wisc.edu

The abstract for this article can be found in this issue, following the table of contents.

DOI:10.1175/BAMS-D-14-00007.1

A supplement to this article is available online (10.1175/BAMS-D-14-00007.2)

In final form 15 April 2015

©2016 American Meteorological Society

Cooperative Institute for Research in the Atmosphere (CIARA) at Colorado State University, and the Cooperative Institute for Mesoscale Meteorological Studies (CIMMS) at the University of Oklahoma, as well as the National Aeronautics and Space Administration (NASA), the National Environmental Satellite, Data, and Information Service (NESDIS), and the National Weather Service (NWS).

The second activity, which works together with the GOES-R3 program, is the Algorithm Working Group (AWG). While both activities involve algorithm development and many of the same organizations, the AWG instead develops, validates, and delivers primarily level 2 products (i.e., derived from level-1b-calibrated and geolocated measurements) for GOES-R Ground Segment (GS) capabilities. The AWG comprises the Application and Development Teams; the Algorithm Integration Team (AIT)—the primary interface between the Application and Development Teams and the GOES-R GS team; the Calibration/Validation (Cal/Val) Team, which works with the GOES-R Cal/Val Working Group and oversees the development and implementation of GOES-R instrument calibration; and the Proxy Data Team. The latter produces, evaluates, and delivers proxy instrument datasets directly to the Application and Development Teams, the AIT, and the GS team.

The third activity is the GOES-R Proving Ground (PG) program, which is a collaboration among many of the same organizations but is focused on providing users with early experience with GOES-R capabilities in an operational setting with the goal of increasing user readiness prior to launch (Goodman et al. 2012). A strong component of the PG program is transitioning research to operations and providing valuable feedback to researchers working under the GOES-R3 program and the AWG. Through this program a variety of ABI products are being supplied to the Advanced Weather Interactive Processing System (AWIPS) for user training. AWIPS is the primary means by which NWS forecasters view and analyze model forecast, satellite, and conventional data.

A common thread throughout all GOES-R activities is the use of proxy satellite data. These data are needed particularly to prepare for the ABI since it has no counterpart in orbit from which to develop and validate algorithms (this was true until October 2014, when the advanced imager on Japan's *Himawari-8* satellite, which is based on the ABI design, was launched). Proxy Data Teams at CIARA, CIMSS, and the NOAA/NESDIS/Center for Satellite Applications and Research (STAR) have been most active in producing proxy ABI data, both from observations and

model simulations with some even in real time. These data play an important role in developing and evaluating ABI product algorithms, testing user ingest and data-handling systems so that users can transition from the current GOES-variable (i.e., GVAR) data format to the future GOES-R Rebroadcast (GRB) data stream, measuring the effects of changes in instrument capabilities on ABI products, and training users through PG activities. In the latter, participants in the 2011 NOAA Hazardous Weather Testbed (HWT) Spring Experiment found synthetic ABI imagery to be invaluable during their forecasts (e.g., Bikos et al. 2012). In all cases, the realistic representation of clouds and other atmospheric features in the proxy datasets made them very useful for satellite demonstration purposes and for evaluating the accuracy of NWP models.

This article highlights our continuing efforts to supply synthetic ABI products to the GOES-R program but within a real-time environment and including product evaluation to prepare users for some of the new products (Schmit et al. 2005). First, the NWP models used in the real-time proxy ABI processing system are described. This is followed by how the proxy ABI products are generated and tested, including progress in our goal of introducing these products into AWIPS II—the NWS's next generation of AWIPS. The capabilities of the real-time system, including product evaluation using current GOES data and model fidelity using Aerosol Robotic Network (AERONET) data, are then shown for three high-impact events: the 2014 Pacific Northwest fires; the 2013 Moore, Oklahoma, tornado; and Hurricane Sandy.

ATMOSPHERIC MODELING. The Weather Research and Forecasting (WRF) Model coupled with chemistry (WRF-Chem) based on the Advanced Research WRF dynamical core (ARW) is the primary regional-scale atmospheric model we use to supply forecasts for proxy ABI data production in real time. Compared to earlier simulations during this project using the ARW Model, the ability to simulate aerosols with WRF-Chem allows simulations of smoke from wildfire and dust events, as well as the effects of aerosol scattering from sea salt and sulfate aerosols for testing ABI aerosol algorithms.

Each day, a 36-h forecast initialized at 0000 UTC is run for the conterminous United States (CONUS) as defined in the GOES-R Product Definition and Users' Guide (PUG; Horne 2014) using WRF-Chem V3.3.1 (Grell et al. 2005) with the Goddard Chemistry Aerosol Radiation and Transport (GOCART) aerosol scheme (Chin et al. 2000, 2002) at 8-km horizontal

grid spacing and with 34 vertical layers. Despite the relatively coarse horizontal resolution, convective clouds are explicitly forecasted so that signatures of fair weather cumulus and deep convective clouds can be included in the radiative transfer model (RTM) calculations. Model grid size/spacing and the choice of the simple GOCART aerosol scheme were based on the constraints of the real-time production cycle. However, these constraints are not expected to prevent the production of realistic datasets.

The main computer system used to generate the WRF-Chem forecasts is the Joint Center for Satellite Data Assimilation (JCSDA) Supercomputer for Satellite Simulation and Data Assimilation Studies (S4). The S4's purpose is to transfer satellite data assimilation and related science (including GOES-R) research results to operations. It is located at the Space Science and Engineering Center (SSEC) at the University of Wisconsin–Madison and had a significant upgrade in 2014 that effectively doubled its compute power and added 1.3 PB of storage.

Subgrid-scale processes in the WRF-Chem model runs are parameterized using the Thompson bulk microphysics scheme (Thompson et al. 2008), the Mellor–Yamada–Janjić planetary boundary layer scheme (Janjić 1994), the Rapid Radiative Transfer Model longwave scheme (RRTM; Mlawer et al. 1997), the Dudhia shortwave scheme (Dudhia 1989), and the unified Noah land surface model for surface heat and moisture fluxes. No cumulus parameterization is used; therefore, all clouds are explicitly predicted by the microphysics scheme. The Thompson scheme predicts cloud water, cloud ice, rain, snow, and

graupel mixing ratios, as well as cloud ice number concentration.

Meteorological initial and lateral boundary conditions (LBCs) come from the National Centers for Environmental Prediction (NCEP) Global Forecast System (GFS). Aerosol initial conditions and LBCs are obtained from the Real-Time Air Quality Modeling System (RAQMS) 1° × 1° global analysis/forecast cycles run daily at CIMSS. RAQMS is a unified (stratosphere–troposphere), online (meteorological, chemical, and aerosol) modeling system that has been developed for assimilating satellite observations of atmospheric chemical and aerosol composition (Pierce et al. 2007, 2009; Verma et al. 2009; McMillan et al. 2010; Dupont et al. 2012; Natarajan et al. 2012). RAQMS assimilates near-real-time (NRT) stratospheric ozone profiles from the Microwave Limb Sounder (MLS) and total column ozone from the Ozone Monitoring Instrument (OMI) on board the NASA *Aura* satellite. RAQMS also assimilates NRT aerosol optical depth (AOD) from the Moderate Resolution Imaging Spectroradiometer (MODIS) instrument on board the NASA *Terra* and *Aqua* satellites. During the chemical and aerosol assimilation cycle the RAQMS meteorological forecasts are reinitialized from NOAA GFS analyses at 6-h intervals.

The WRF-Chem forecasts use high-resolution CONUS anthropogenic aerosol precursor emissions based upon the U.S. EPA's 2005 National Emissions Inventory (NEI-2005). The forecasts also include biomass burning emissions from the preceding day produced from Wild Fire Automated Biomass Burning Algorithm wildfire products (Koltunov et al. 2012).

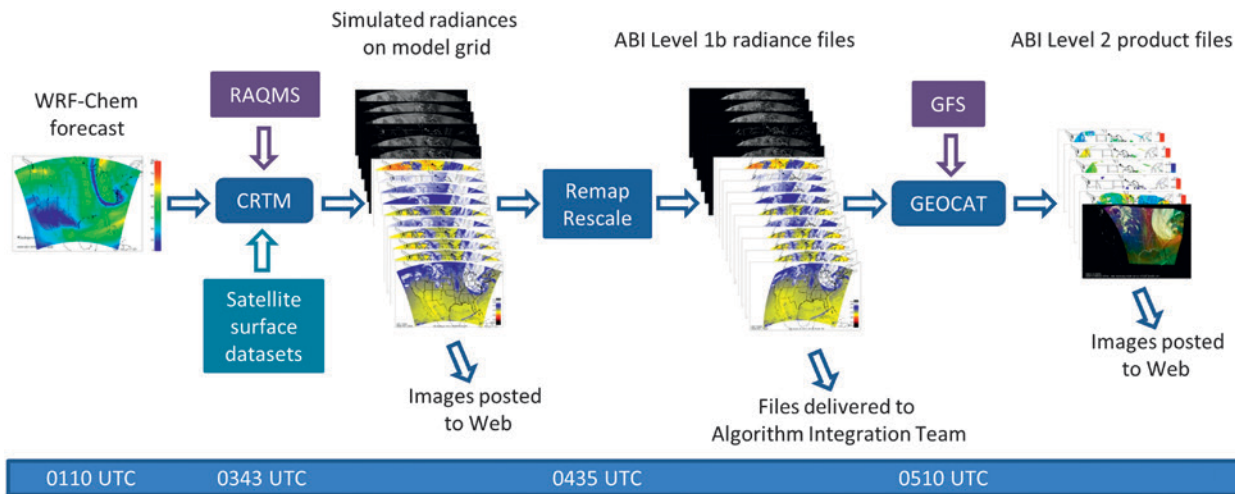


FIG. 1. Production flow for generating real-time simulated ABI level 1b radiance products and level 2 products. Approximate processing times are indicated at bottom of figure. Generation of level 2 products is in semi-real time based on availability of GFS data required by the ABI algorithms in GEOCAT.

TABLE 1. Characteristics of the ABI and proxy bands from the GOES-13 sounder and imager. Here, IGFOV = instantaneous geometric field of view.
 [Adapted from Schmit et al. (2005).]

ABI band	Central wave-length (μm)	Nominal subsatellite GFOV (km)	Principal use	GOES-13 sounder band	Central wave-length (μm)	Nominal subsatellite IGFOV (km)	GOES-13 imager band	Central wave-length (μm)	Nominal subsatellite IGFOV (km)
1	0.47	1	Daytime continental aerosol						
2	0.64	0.5	Daytime clouds; fog; winds	19	0.70	10	1	0.65	1
3	0.865	1	Daytime vegetation; burn scar						
4	1.378	2	Daytime cirrus						
5	1.61	1	Cloud properties						
6	2.25	2	Cloud properties						
7	3.90	2	Fire; night fog	17	3.98	10	2	3.9	4
8	6.19	2	High-level water vapor	12	6.5	10	3	6.5	4
9	6.95	2	Midlevel water vapor	11	7.02	10			
10	7.34	2	Low-level water vapor	10	7.43	10			
11	8.5	2	Cloud phase; stability						
12	9.61	2	Column ozone	9	9.71	10			
13	10.35	2	Surface; clouds				4	10.7	4
14	11.2	2	SST; clouds	8	11.03	10			
15	12.3	2	SST	7	12.02	10			
16	13.3	2	Cloud height; low-level temperature	5	13.37	10	6	13.3	4

PROXY ABI DATA GENERATION AND EVALUATION.

This section describes how the WRF-Chem and RAQMS 3D model forecast fields are transformed into ABI radiances and products, and how the simulated products are compared against *GOES-13* data. Figure 1 illustrates the basic flow of the real-time generation of simulated data. The processing of hourly GOES observations in real time follows a similar path; however, the evaluation phase is currently not done in real time.

The simulation processing path first takes model output from the last 24 h of a given forecast and uses the JCSDA's Community Radiative Transfer Model (CRTM) V2.1 to compute hourly ABI radiances for all 16 visible and infrared bands (see Table 1) at each model grid point. Profiles of ozone concentration needed by the CRTM are obtained from RAQMS forecasts, which are also used to specify temperature and water vapor above the WRF-Chem model top of 50 hPa. The CRTM uses the GOCART aerosol specification model for aerosol optical properties, which provides consistency between the types of aerosols predicted by WRF-Chem and the computed radiances.

Other properties needed by the CRTM to generate realistic ABI imagery are land surface emissivity and reflectance datasets derived from MODIS observations. The CRTM user-defined land surface emissivity for the ABI infrared bands (7–16) is obtained by convolving the high spectral resolution University of Wisconsin (UW) Baseline Fit (BF) emissivity database with the ABI spectral response functions (Seemann et al. 2008). Land surface reflectivity for the ABI solar bands (1–6) is based on 16-day running-average MODIS bidirectional reflectance distribution function/albedo products produced in real time at the SSEC using direct-broadcast data (Shuai et al. 2013).

Once the simulated ABI brightness temperatures and reflectances are computed, images are posted online (http://cimss.ssec.wisc.edu/goes_r/proving-ground/wrf_chem_abi/wrf_chem_abi.html).

What sets these proxy ABI datasets apart is that the level 1b radiance products are reproduced as close as possible to what they will actually be in the GRB data flow. This includes storing the data in Network Common Data Format (netCDF) files that conform to Climate and Forecast (CF) metadata conventions and incorporating the ABI fixed grid coordinates and scanning geometry. The ABI fixed grid is a new feature in GOES navigation that eliminates navigational jitter by putting the observations on the same reference latitude–longitude grid at each observation time, similar to what is currently done with the Spinning Enhanced Visible and Infrared Imager (SEVIRI) on

the European Meteosat satellites (Horne 2014). Fixed grid resolutions for each ABI channel are shown in Table 1.

Generation and testing of the proxy ABI datasets were important in defining certain aspects of the level 1b file structure that contributed to the ABI PUG and the development of the AWG Imagery team Algorithm Theoretical Basis Document. However, the level 1b files that were produced differ somewhat from those defined in the PUG in that we use netCDF version 3 rather than version 4 and all simulated ABI radiance data are remapped from the WRF-Chem model grid to the lowest-resolution (i.e., 2 km) fixed grid.

The simulated ABI level 1b radiance files are used in three ways: 1) delivered in real time to the GOES-R AIT as a means of validating baseline products within their comprehensive algorithm framework, 2) processed through the Geostationary Cloud Algorithm Testbed (GEOCAT) to create ABI baseline products for verification and use in AWIPS II, and 3) evaluated directly against current GOES imagery and products. Originally developed by the GOES-R AWG Cloud Application Team as a flexible cloud retrieval algorithm development tool, GEOCAT accepts a variety of other ABI algorithms (e.g., fire detection, soundings, aerosols) and can read ABI level 1b data files as well (Martin 2007). Table 2 shows the ABI baseline and option 2 products currently produced by GEOCAT. Our real-time system is currently processing ABI cloud and legacy sounding baseline products (Xie et al. 2013), total ozone option 2 products, and red–green–blue (RGB) airmass imagery. Images of these products are made available online (http://cimss.ssec.wisc.edu/goes_r/proving-ground/wrf_chem_abi/ABI-PRODUCTS/wrf_chem_abi_prod.html).

Important strides have been taken in making these simulated products and imagery available to forecasters within AWIPS II. Development work is being done on an AWIPS II beta release built on the NCEP 14.1 branch of source code. Conversion of the ABI level 1b radiance files and level 2 product files into a format accepted by AWIPS II is accomplished using a remapping tool written in the Interactive Data Language (IDL). However, this approach is somewhat inefficient and alternative ways of converting these files for real-time applications are being considered.

The GOES sounder is the main source of evaluation for the simulated ABI products since it is the closest observational proxy to the ABI over the United States. Although it has much coarser spatial resolution than the GOES imager, its wide spectral range covers 9 of the 16 ABI channels (see Table 1). The spectral characteristics for the overlapping channels

TABLE 2. Summary of ABI products produced from GEOCAT, the real-time simulation system, and GOES sounder.

Baseline products	GEOCAT	Real-time simulation	Real-time GOES sounder
Cloud and moisture imagery	✓	✓	✓
Radiances	✓	✓	✓
Aerosol detection (including smoke and dust)	✓		
Aerosol optical depth	✓		
Volcanic ash detection and height	✓		
Cloud optical depth	✓		
Cloud particle size	✓		
Cloud-top phase	✓	✓	
Cloud-top height	✓	✓	
Cloud-top pressure	✓	✓	✓
Cloud-top temperature	✓	✓	
Hurricane intensity			
Rainfall rate and quantitative precipitation estimation			
Legacy vertical moisture profile	✓	✓	
Legacy vertical temperature profile	✓	✓	
Derived stability indices	✓	✓	✓
Total precipitable water	✓	✓	✓
Clear-sky mask	✓	✓	✓
Downward shortwave radiation at surface			
Fire/hot spot characterization	✓		
Land surface (skin) temperature			
Sea surface (skin) temperature			
Reflected shortwave radiance at top of the atmosphere			
Snow cover			
Derived motion winds	✓		
Selected option 2 products			
Aerosol particle size	✓		
Ozone total	✓	✓	✓
Cloud type	✓	✓	
Cloud ice water path	✓		
Cloud layers and heights	✓		
Cloud liquid water	✓		
SO ₂ detection	✓		
Low cloud and fog	✓		
Other derived products			
RGB air mass		✓	
True-color imagery		✓	

have some differences for each sensor; however, the biases due to these spectral differences can be estimated with RTM calculations using a *U.S. Standard Atmosphere, 1976* under clear-sky conditions. The *GOES-13* sounder was chosen specifically because of the location assumed in the generation of the *GOES-R* proxy radiances (75°W).

GOES-13 sounder data are collected in real time at the SSEC, roughly 15 min after each hour. These data are then converted from Man Computer Interactive Data Access System (McIDAS) area files into netCDF-3 files. At the same time, SSEC produces experimental real-time products derived from sounder data (Schmit et al. 2008). A subset of these data, namely lifted index, convective available potential energy (CAPE), cloud-top pressure, total precipitable water (TPW), and the cloud mask, is then converted into netCDF-3 files for use in our validation system. The last step involves remapping the sounder data onto the ABI 2-km fixed grid and generating netCDF-3 files. The remapping enables direct spatial comparisons between the *GOES* sounder data and the simulated ABI data.

Evaluating simulated ABI data using *GOES-13* data is complicated by NWP model errors, CRTM errors (including surface radiative property uncertainties), algorithm differences, and spectral differences between the simulated ABI and *GOES-13* sounder channels. Despite these challenges, we have found that evaluating the simulated ABI imagery in this way has been extremely useful in identifying key issues with the CRTM and WRF-Chem models, including errors in the microphysics parameterizations and in how the CRTM handles surface radiative properties and spectral regions where both solar radiation and infrared emission occur.

While we have experience evaluating both synthetic imagery and derived products (Otkin et al. 2007; Otkin and Greenwald 2008; Otkin et al. 2009; Cintineo et al. 2014; Lee et al. 2014), this study focuses on the ABI-derived products. The approach in dealing with one of the largest sources of NWP model errors, namely displacement errors in the

location of the simulated cloud fields, is to simply compare the products at grid points where both simulated ABI data and *GOES-13* sounder data are determined to be clear sky or cloudy sky. Whether a particular grid point is deemed clear sky or cloudy sky is based on the ABI baseline cloud mask produced from GEOCAT for the simulated data and conversely the operational *GOES-13* sounder cloud mask for the observations.

CASE STUDY DEMONSTRATIONS. At 0909 Pacific daylight time (PDT) on Friday, 11 July 2014, the NWS office in Pendleton, Oregon, issued a fire weather watch for central Oregon that extended until Sunday evening, 13 July. This watch was upgraded to a red flag warning at 1437 PDT on Saturday, 12 July, because of hot and dry conditions and thunderstorms over Oregon with abundant lightning and little precipitation. Dry lightning strikes from these storms led to the ignition of a number of large wildfires in Oregon, Washington, and Idaho on Monday, 14 July, that led to significant property loss and adverse health effects associated with heavy smoke plumes across the Pacific Northwest, which prompted the governors of Washington and Oregon to declare states of emergency. These fires included the Black Rock fire in northern Oregon, the Buzzard Complex in eastern Oregon, the Carlton Complex in northern Washington, and the Whiskey Complex in western Idaho. The Carlton Complex burned 256,108 acres and was the largest wildfire in Washington's recorded

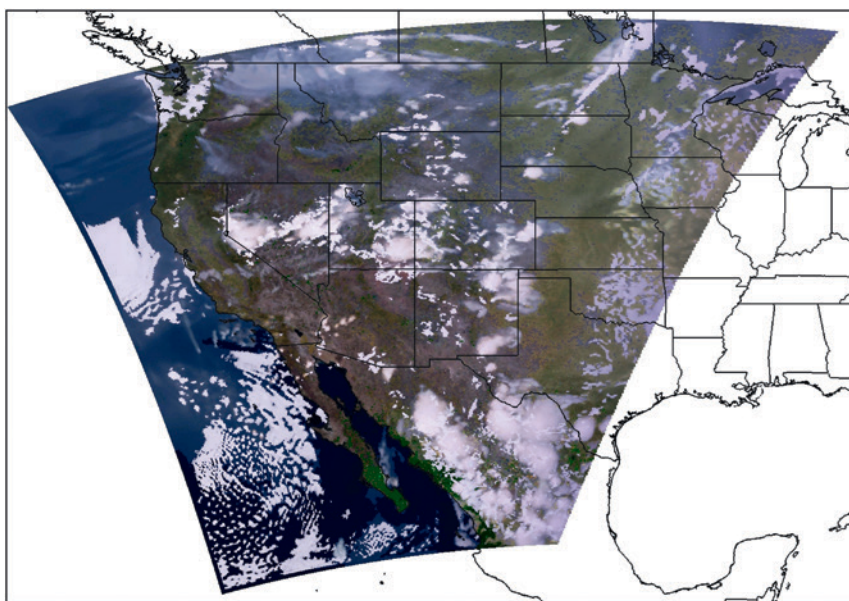


FIG. 2. Simulated ABI true-color imagery for the Pacific Northwest wildfires at 0100 UTC 19 Jul 2014.

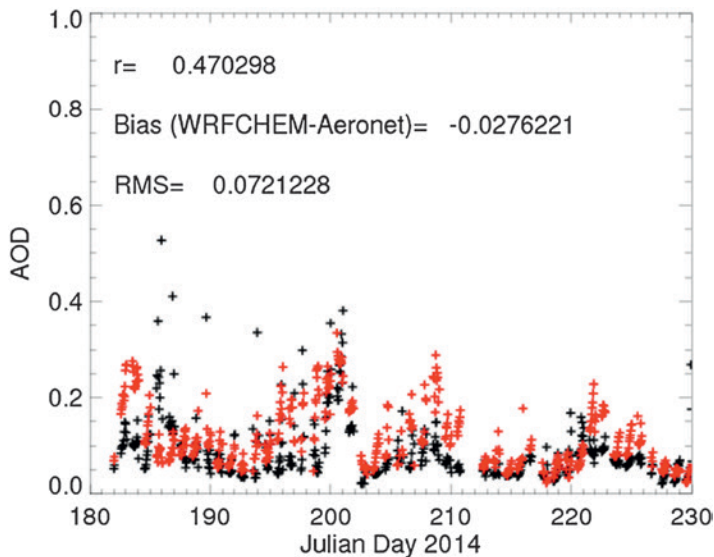


FIG. 3. Time series of observed (red) and simulated (black) composite AOD results during the 2014 Colorado DRAGON campaign. Julian day 200 corresponds to 19 Jul 2014.

history. The National Wildfire Coordinating Group (NWCG; www.nwcg.gov) provides detailed summaries of these and other U.S. wildfires through their Incident information System (INCIWEB; <http://inciweb.nwcg.gov>).

The magnitude of these wildfires provides a good opportunity to evaluate the fidelity of the aerosol component of our modeling system and highlight the ability of the ABI to observe the spread of wildfire smoke. Figure 2 shows a synthetic true-color image valid at 0100 UTC 19 July 2014 (1800 PDT 18 July 2014), which corresponds to the period of peak Pacific Northwest wildfire activity during 2014. This image was generated using simulated ABI red, blue, and near-infrared (NIR) bands along with a lookup table (LUT) for the green band that was generated from a composite of diurnally resolved simulated ABI scenes following the approach outlined by Miller et al. (2012). We used ABI viewing geometry and MODIS

ing Information on Surface Conditions from Column and Vertically Resolved Observations Relevant to Air Quality (DISCOVER-AQ; <http://discover-aq.larc.nasa.gov/>) campaign provides a unique opportunity to assess the fidelity of our modeled aerosol optical depths. Figure 3 shows a time series of the composite observed and simulated AOD results during the Colorado DRAGON campaign (1 July–18 August 2014). The simulated AOD has been filtered by the simulated cloud optical depth (COT < 1.0) to account for errors in cloud predictions. The simulated AOD captures the daily variations of the observed aerosol loading fairly well ($r = 0.47$, bias = -0.03 , rms error = 0.07) when composited over the DRAGON network, including the enhanced AOD on 19 July (Julian day 200) associated with the transport of smoke from the Pacific Northwest wildfires. Comparison of individual observed and cloud-cleared simulated AOD results reveals similar skill ($r = 0.46$, bias = -0.02 , rms error = 0.08) and shows that while the simulated AOD is systematically low compared to the DRAGON observations the majority of data points are within a factor of about 2 (see Fig. ES1 in the online supplement to this paper).

2013 Moore, Oklahoma, tornado. The tornado that struck Moore, Oklahoma, on 20 May 2013 was rated as a category 5 event on the enhanced Fujita scale (EF5), had a maximum width of 2.1 km, and stayed on the ground for 39 min. Twenty-four

TABLE 3. Lifted index (LI), CAPE, and TPW derived from WRF-Chem model forecast, proxy ABI retrievals from synthetic brightness temperatures, and observations for Dallas–Fort Worth at 1800 UTC 20 May 2013.

	LI	CAPE (J kg ⁻¹)	TPW (cm)
WRF-Chem model	-6.7	1,757	3.4
Proxy ABI retrieval	-6.9	1,848	3.5
Raob	-8	3,258	3.0
GOES observation	-7.7	3,350	3.8

people lost their lives and another 377 were injured. Very early signs of the possibility for severe weather in this area prompted the local NWS office in Norman, Oklahoma, to alert the public five days earlier of an enhanced risk for severe weather. In addition to high wind shear, another ingredient that favored the development of supercells was the very unstable air mass ahead of an approaching cold front to the north and a dryline to the west, with 19°–20°C dewpoints, temperatures in the upper 20s (°C), and CAPE of over 3,500 J kg⁻¹.

Observations made by the *GOES-13* sounder within an hour before convection began on 20 May

indicated CAPE of over 3,000 J kg⁻¹ across the entire eastern half of Texas and into Oklahoma with values as high as 5,000 J kg⁻¹ along a thin strip running parallel with the dryline (see Fig. ES2 in the online supplement). These observations were consistent with an observed value of 3,258 J kg⁻¹ from a special 1800 UTC sounding at Dallas–Fort Worth, Texas (Table 3). Although the proxy ABI CAPE products were biased about a factor of 2 lower than the observations (Fig. 4), they did show remarkably similar spatial features to the *GOES* observations (cf. Figs. 5 and ES2). This bias was due to underpredictions of CAPE by the WRF-Chem forecast and not the ABI

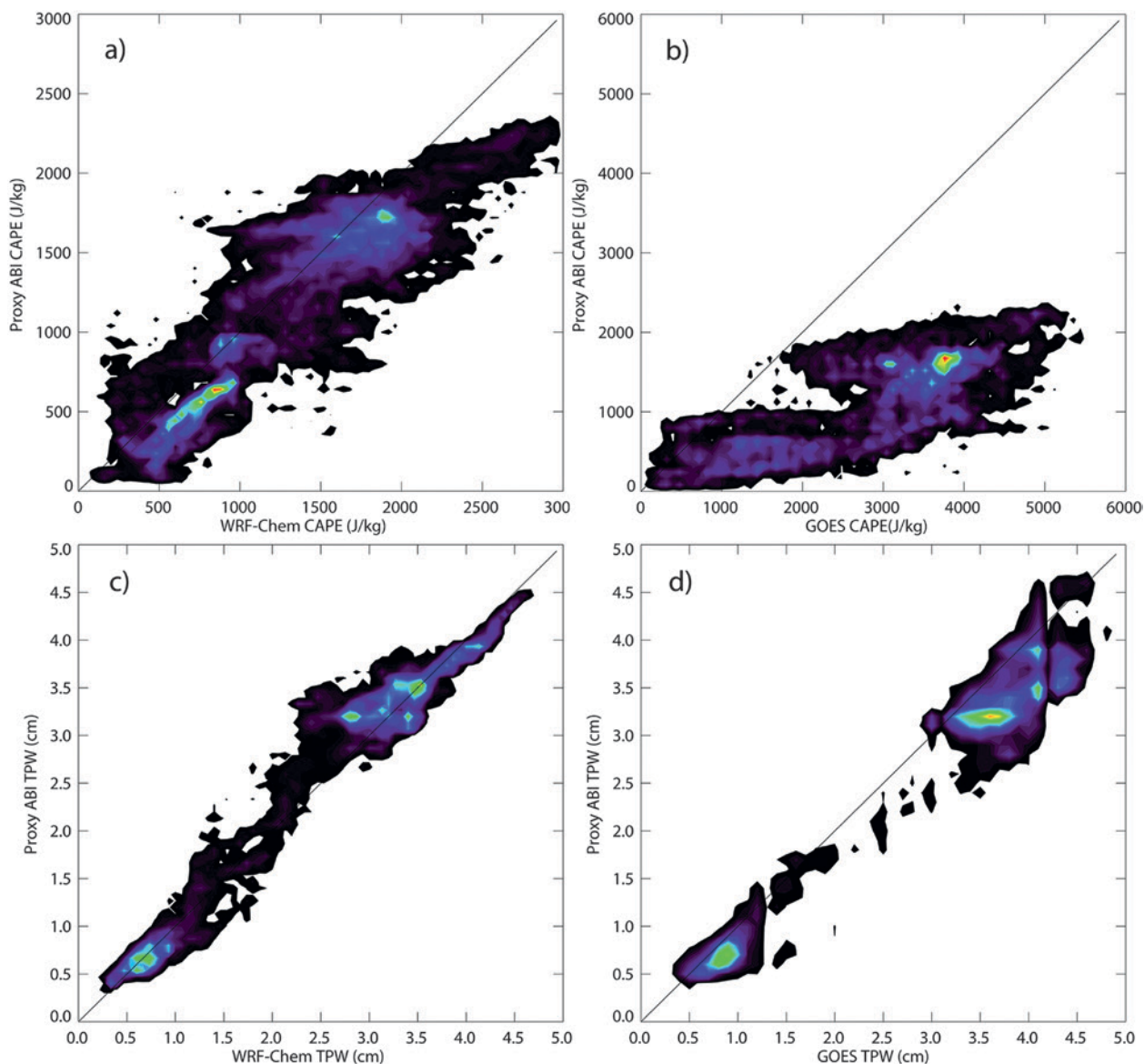


FIG. 4. Density scatterplots of (a) WRF-Chem model and retrieved ABI CAPE products, (b) retrieved proxy ABI and *GOES-13* sounder CAPE products, (c) WRF-Chem model and retrieved proxy ABI TPW products, and (d) retrieved proxy ABI and *GOES-13* sounder TPW products for 1800 UTC 20 May 2013.

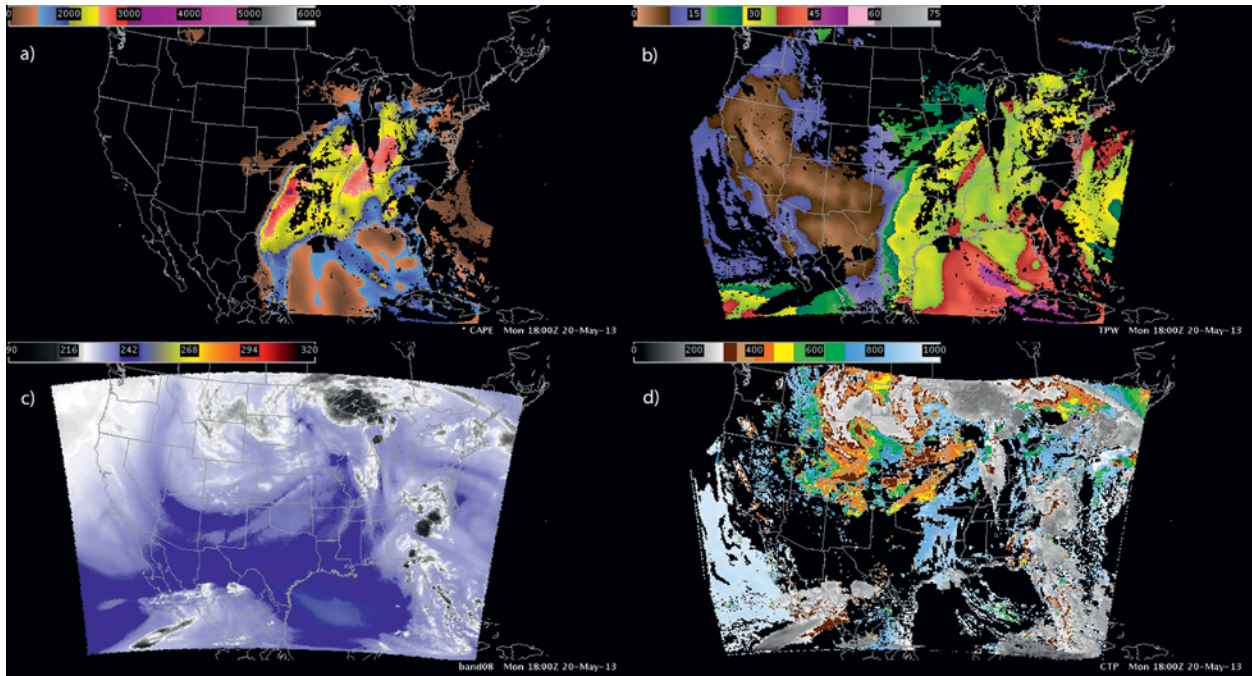


FIG. 5. AWIPS II four-panel display of simulated ABI imagery and products for 1800 UTC 20 May 2013: (a) CAPE, labels at 0, 2,000, 3,000, 4,000, 5,000, and 6,000 J kg^{-1} ; (b) TPW, labels at 0, 15, 30, 45, 60, and 75 cm; (c) band 8 ($6.19 \mu\text{m}$) imagery (BT), labels at 90, 216, 242, 268, 294, and 320 K; and (d) CTP, labels at 0, 200, 400, 600, 800, and 1,000 hPa.

temperature–humidity profile algorithm (Fig. 4), possibly caused by the forecast producing surface temperatures that were cooler than observed (Fig. 6).

Evidence of widespread high moisture content at low levels was seen in the *GOES-13* sounder retrievals of TPW (see Fig. ES2) with values in some areas of Texas and Oklahoma exceeding 4 cm. Comparison to the 1800 UTC sounding, however, shows these retrievals were slightly too high (Table 3). Again, the proxy ABI products reproduced the spatial distribution of TPW but in this case were actually in better agreement with the radiosonde than the *GOES-13* retrievals, which were too moist at the lowest levels of the atmosphere (see Fig. 6).

From *GOES* visible imagery, signs of convection appeared along the line of exceedingly high CAPE observed by the *GOES* sounder in southern Oklahoma and northwest Texas as early as 1815 UTC. The model forecast, on the other hand, lagged the actual start of the convection by about 3 h but did produce it in the correct location. Figure 7 shows the synthetic ABI products, including cloud-top pressure (CTP), at 2300 UTC as they appear within AWIPS II. The CTPs of the simulated convective clouds over a 5-h period after convection started were found to agree well with the *GOES-13* sounder CTP products from 3 h earlier also over a 5-h period (see Fig. 8). This

means that despite the delay in the onset of deep convection, the WRF Model forecast did a good job of predicting the convective environment that led to the tornado outbreak and gives more confidence in the proxy data products to help forecasters learn more about the capabilities of the ABI. Animations of the evolution of these storms from both simulated and observed perspectives are available in Figs. ES3 and ES4, respectively, in the online supplement.

Hurricane Sandy. A category 3 storm at its peak intensity, Sandy was the second costliest hurricane in U.S. history and largest Atlantic hurricane on record. It formed in the western Caribbean Sea on 22 October 2012 and made landfall along the New Jersey coast seven days later as a post-tropical cyclone with hurricane force winds. Although Sandy occurred before the real-time system was put in place, the simulation was run in the same real-time configuration consisting of a multiday series of retrospective short-range forecasts. To evaluate the proxy ABI datasets, we focused on the latter stages of Hurricane Sandy and ran the WRF-Chem model in a series of separate 36-h forecasts, each beginning at 0000 UTC, the first of which began at 0000 UTC 26 October and the last ending at 1200 UTC 1 November. Only forecasts for 1200 UTC on day 1 to 1200 UTC on day 2 were used in the analyses.

Cloud and sounding products were used in the analysis to reveal information about the large-scale environment and cloud characteristics of Sandy. Because of its ability to identify jet streams, rapid cyclogenesis, and other atmospheric phenomena, one promising product that can be derived from ABI imagery is RGB air mass. This color composite consists of the red component as the brightness temperature (BT) difference between a high-level water vapor band ($6.19\ \mu\text{m}$ for the ABI and $6.5\ \mu\text{m}$ for the GOES sounder) and a low-level water vapor band ($7.34\ \mu\text{m}$ for the ABI and $7.43\ \mu\text{m}$ for the GOES sounder); the green component as the BT difference between the ozone band ($3.90\ \mu\text{m}$ for the ABI and $3.98\ \mu\text{m}$ for the GOES sounder) and an IR window band ($11.2\ \mu\text{m}$ for the ABI and $11.03\ \mu\text{m}$ for the GOES sounder); and the blue component as the high-level water vapor band BT. Other typical applications for the RGB air mass include locating areas of high potential vorticity and, as the product's name implies, differentiating between air mass types. The latter has been found to be useful for hurricane forecasters. Indeed, the Regional and Mesoscale Meteorology Branch (RAMMB) of CIRA is supplying this experimental product derived from SEVIRI and GOES sounder data to the National Hurricane Center (Goodman et al. 2012).

Figure 9 shows RGB air-mass fields derived from simulated ABI imagery and GOES-13 sounder imagery at two different stages of Sandy's life cycle: as a category 1 hurricane a day after reaching its peak intensity and later during landfall (5-day animations of simulated and observed RGB air-mass fields are shown in Fig. ES5 in the online supplement). One thing to bear in mind is that nearly all of the significant color differences, especially in clear-sky regions, seen in Fig. 9 are due to spectral differences between the ABI and GOES-13 sounder (see Table 1). This was confirmed by directly comparing the separate color components

while accounting for spectral differences (see Fig. ES6 in the online supplement). For example, while the cold air mass in the northwest part of the region observed by the sounder shows a bluish color in the observations, it is instead a purplish hue in the simulated ABI imagery. The larger BT difference for the simulated red component, caused by the ABI's colder $6.19\text{-}\mu\text{m}$ channel peaking somewhat higher in the atmosphere than the GOES sounder's $6.5\text{-}\mu\text{m}$ channel, results in a larger contribution of red color to the composite, thus making it appear more purplish in color.

On 26 October the location of the storm is in good agreement with the GOES-13 observations, though the region of thick high clouds (denoted as whitish) and thick midlevel clouds (denoted as light ochre) appears broader than in the observations. While the simulated ABI imagery shows a strong greenish color in the Gulf of Mexico, suggesting an ozone-rich tropical air mass, the observations appear to have a more bluish green hue. Again, this is due to the effects of different spectral characteristics of the ABI and GOES sounder bands that are used

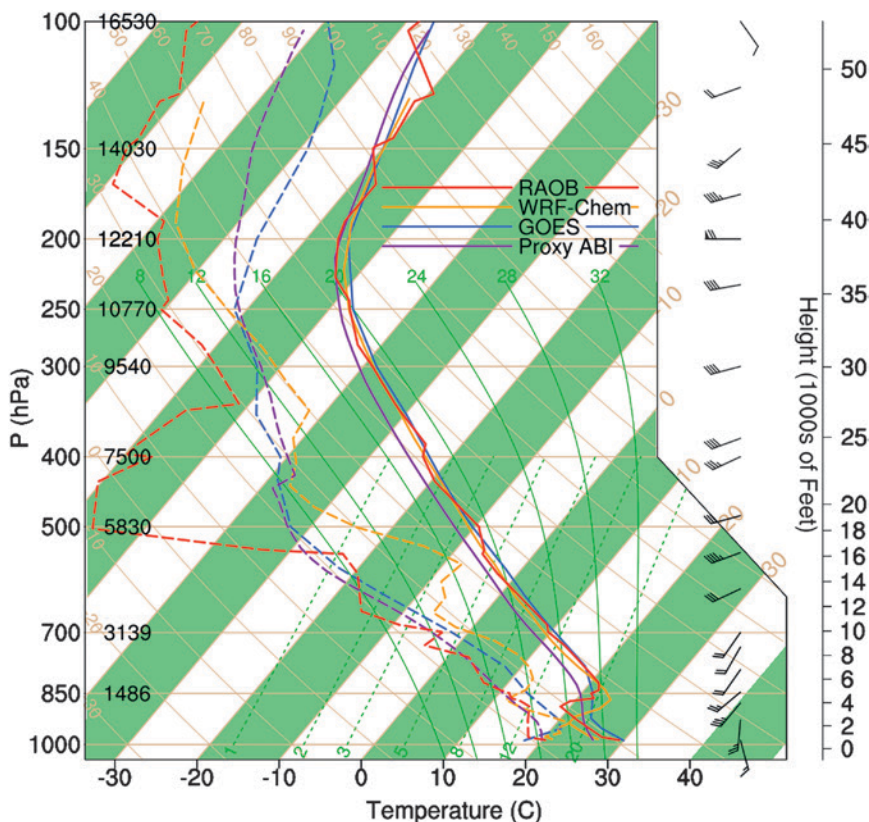


FIG. 6. Skew T -log p diagram of air temperature (solid) and dewpoint temperature (dashed) profiles for the WRF-Chem model, proxy ABI products, GOES-13 sounder products, and radiosonde observations (raobs) at 1800 UTC 20 May 2013 near Dallas-Fort Worth. Wind barbs are from the radiosonde.

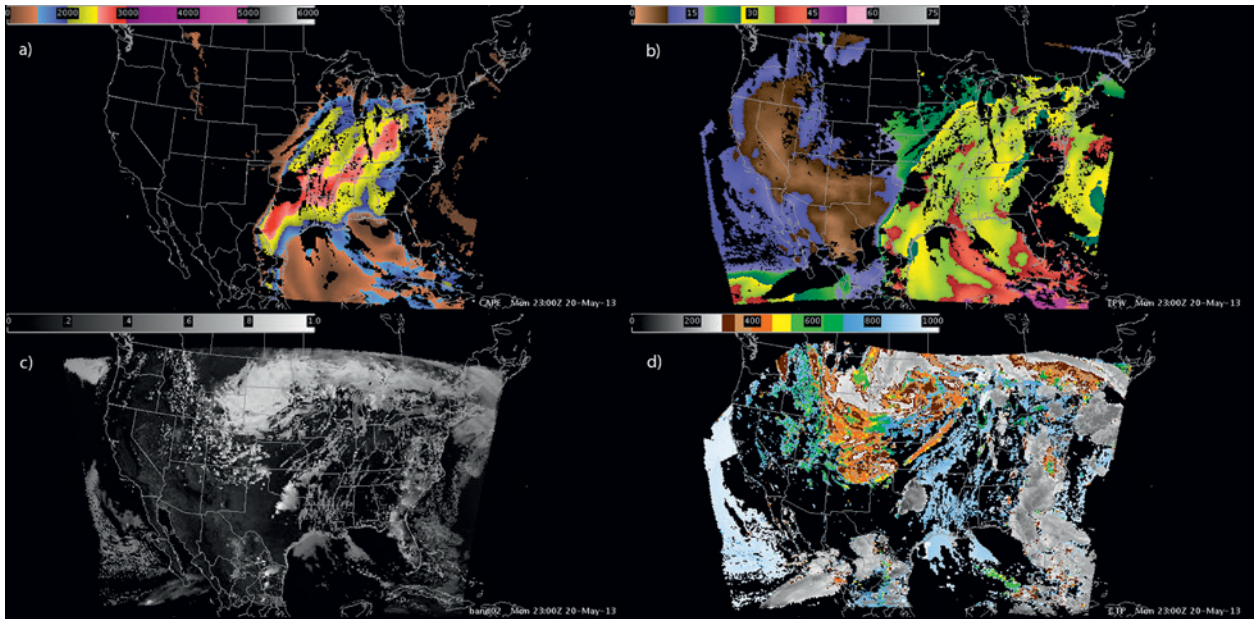


FIG. 7. AWIPS II four-panel display of simulated ABI and products for 2300 UTC 20 May 2013: (a) CAPE, labels at 0, 2,000, 3,000, 4,000, 5,000, and 6,000 J kg^{-1} ; (b) TPW, labels at 0, 15, 30, 45, 60, and 75 cm; (c) band 2 ($0.64 \mu\text{m}$) imagery (albedo), labels at 0, 0.2, 0.4, 0.6, 0.8, and 1.0; and (d) CTP, labels at 0, 200, 400, 600, 800, and 1,000 hPa.

to produce the red and blue components of the RGB airmass imagery and are fully consistent with the expected differences based on clear-sky *U.S. Standard Atmosphere, 1976* RTM calculations.

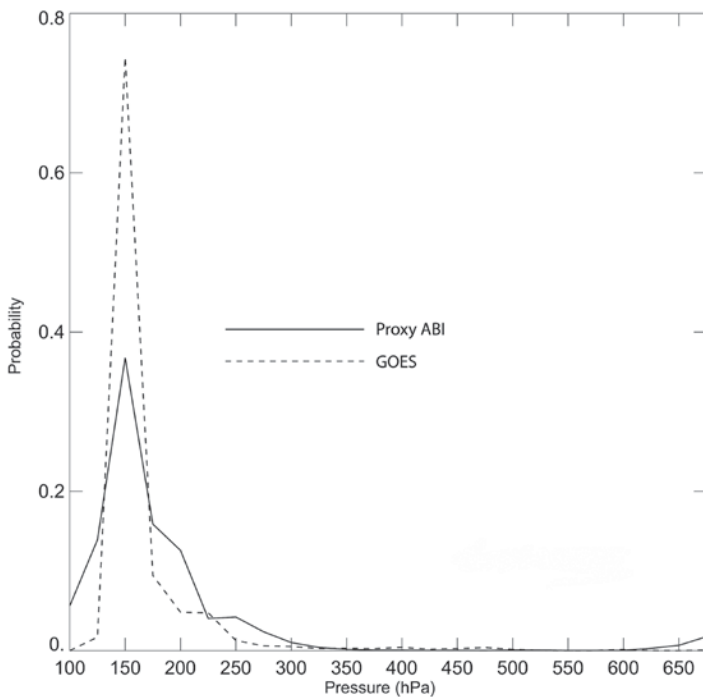


FIG. 8. Probability distribution functions of CTP for deep convection over OK from GOES-13 sounder products from 2000 UTC 20 May to 0100 UTC 21 May 2013 (dashed) and proxy ABI products from 2300 UTC 20 May to 0400 UTC 21 May 2013 (solid).

The most dramatic feature of Sandy as it made landfall was its enormous size. The storm covered the entire northeast United States and affected parts of the Midwest as far west as Milwaukee, Wisconsin.

The extent of the storm and its location were reproduced well by the model forecast. However, the ice clouds appear slightly thicker and higher in the simulated imagery. A distinctly purplish strip located west of the cloud shield across Wisconsin, Iowa, and Illinois in the observations corresponds to the region in between two jets where very dry air is likely descending from the stratosphere. This same feature shows up well in the simulated imagery too but is somewhat maroon in color.

Another prominent feature is the extensive orange-colored region near the southern edge of Sandy's cloud shield that appears in both the simulated imagery and GOES observations. The color suggests very dry air is wrapping around the storm, which is located just north of a strong jet across southern Florida that can be seen in the simulated ABI high-level water vapor imagery for this time period (see Fig. 10).

An ABI product that provides information on the variation of the height of the cloud tops is CTP (Fig. 10). As suggested earlier based on inspection of the

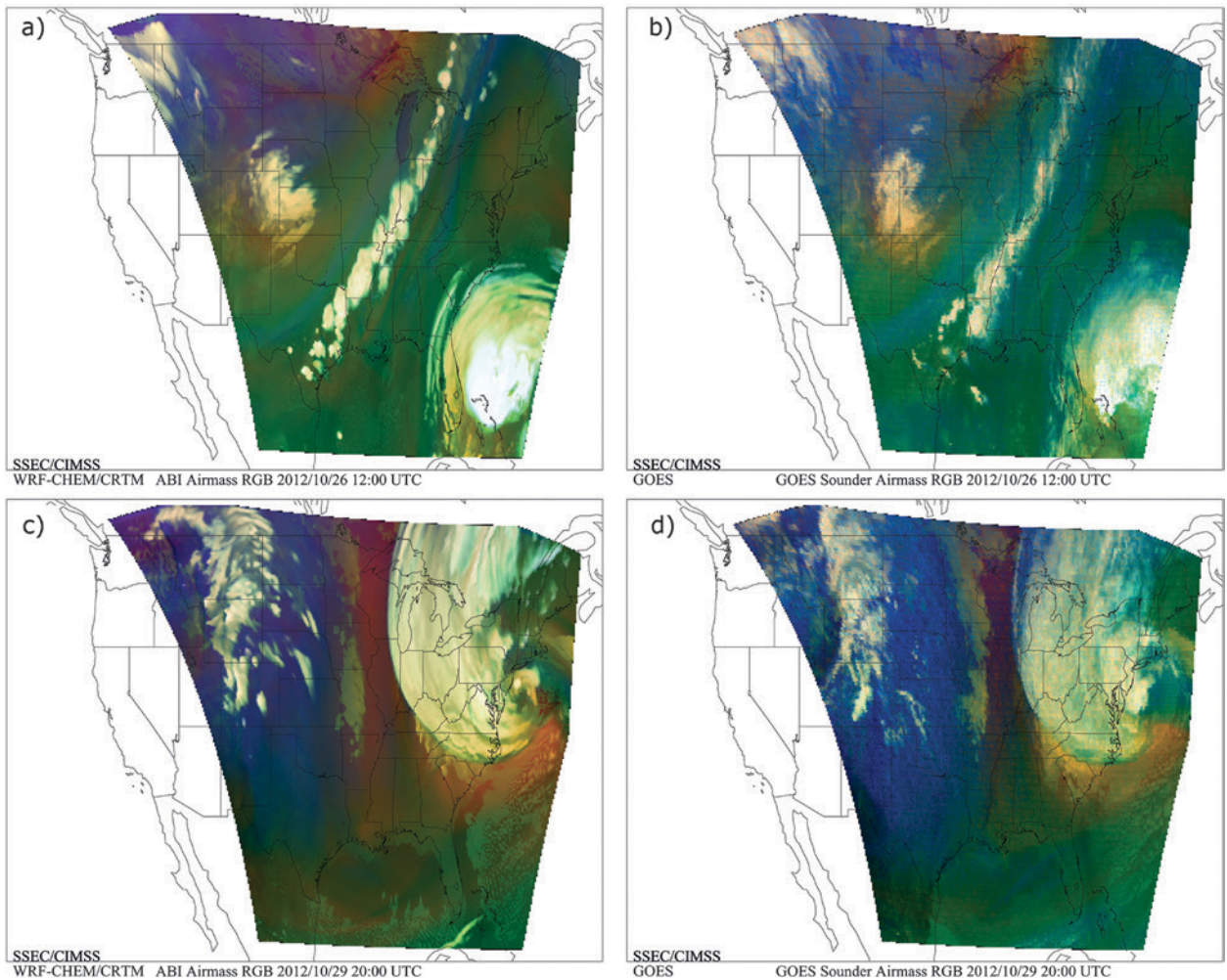


FIG. 9. Simulated (a) ABI- and (b) GOES-13-observed RGB airmass imagery for Hurricane Sandy at 1200 UTC 26 Oct 2012. (c),(d) As in (a),(b), but for 2000 UTC 29 Oct 2012.

simulated ABI RGB airmass imagery, the simulated high clouds associated with the massive ice shield generated by Sandy were located too high in the atmosphere, with CTPs about 50–100 hPa less than the observations (Fig. 11). These differences are largely a result of biases in the WRF-generated cloud heights and not significant errors in the ABI algorithm. The broad region of low-level clouds that formed off the southeastern U.S. coast as a result of advection of cool air over the warmer ocean was captured by the forecast, though the CTPs were on average about 100 hPa less than observed. Whether these differences are the result of forecast errors and/or biases in the satellite retrievals is unclear. However, it is well recognized that satellite infrared sensors have difficulty accurately estimating the heights of low clouds (e.g., Weisz et al. 2007).

Another cloud-top property to investigate is cloud thermodynamic phase. In combination with other

information, this satellite product has been useful in nowcasting icing threats for aviation (Smith et al. 2012). It is derived from the ABI infrared channels for the following categories: warm liquid water, supercooled liquid water, mixed phase, and ice phase (Pavolonis 2010). As expected, most of the clouds directly associated with Sandy are in the ice phase, though significant areas of supercooled liquid water are evident in southern North Carolina and New England (see Fig. 10). However, inspection of the simulated 1.378- μm band of the ABI, a unique channel for a geostationary sensor and a measure of the reflectance of cirrus clouds, shows low reflectance values in isolated areas of southern North Carolina, indicating some of the clouds may have been misidentified as supercooled liquid water. The simulated products compare well to the GOES-13 imager observations except in the regions of supercooled liquid water identified earlier where the observations

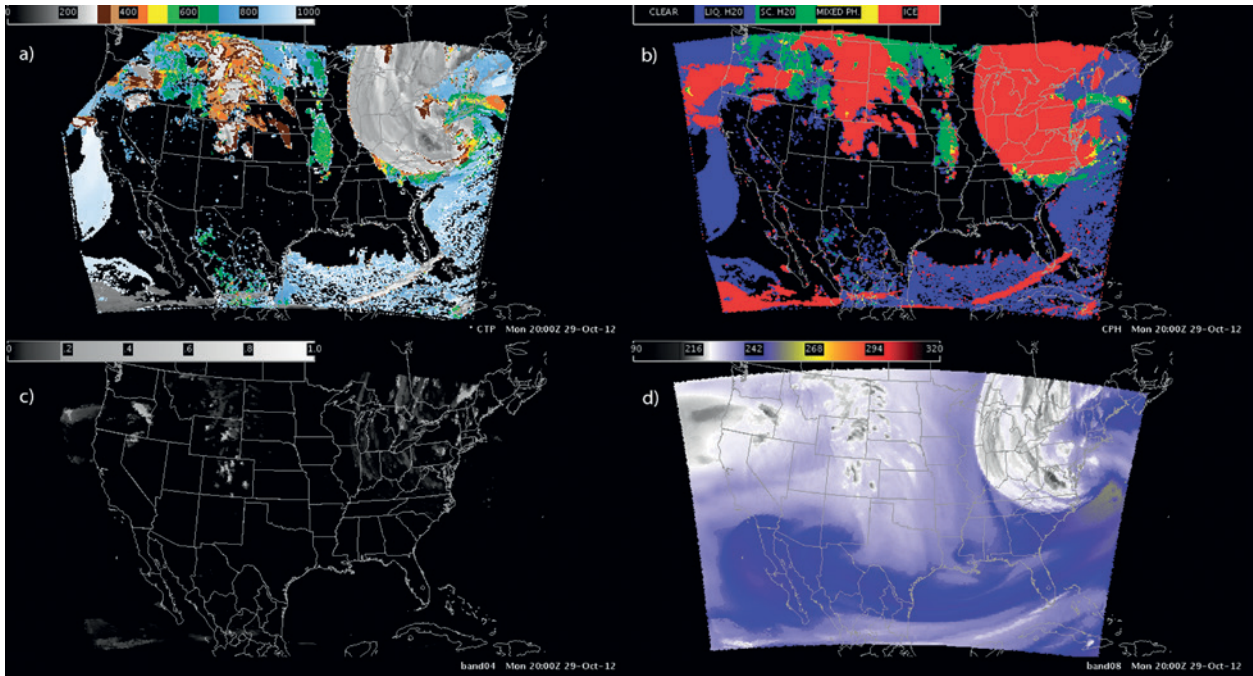


FIG. 10. AWIPS II four-panel display of simulated ABI imagery and products for 2000 UTC 29 Oct 2012: (a) CTP, labels at 0, 200, 400, 600, 800, and 1,000 hPa; (b) cloud thermodynamic phase (CPH), labels for clear, liquid H₂O, supercooled H₂O, mixed phase, and ice; (c) band 4 (1.378 μm) imagery (albedo), labels at 0, 0.2, 0.4, 0.6, 0.8, and 1.0; and (d) band 8 (6.19 μm) imagery (BT), labels at 90, 216, 242, 268, 294, and 320 K.

show instead the prevalence of mixed-phase and ice clouds (Fig. 12).

These results demonstrate that the simulated ABI products evaluated here for hurricane applications are useful as training material for users—a consequence of the WRF-Chem model realistically simulating the overall structure and cloud characteristics of Sandy.

SUMMARY. A simulation system that has been operating nearly continuously for over two years was developed for generating synthetic ABI imagery and derived products in real time over the United States with the main purpose of testing ABI retrieval and visualization algorithms and making these data available to forecasters and other future users of ABI data through GOES-R PG activities. The system is unique in that it simulates all channels of the ABI, uses a high-resolution NWP model with aerosols and a real-time global air-quality model to more accurately represent ozone and aerosols in the synthetic imagery, and provides ABI level 1b radiance files as they will appear in the GRB data stream.

Results from one wildfire and two severe weather case studies have shown that realistic proxy ABI imagery and high quality derived products can be produced by the system. Differences between the simulated AOD and DRAGON observations show

that the simulated AOD is within a factor of 2 of the observations over the Front Range of Colorado and that realistic true-color imagery of smoke can be generated using LUT approaches based on simulated ABI red, blue, and NIR bands, in conjunction with simulated green band radiances. Differences between the simulated data and GOES observations were related more to model forecast errors and/or spectral differences between the ABI and GOES sounder than to inherent ABI algorithm issues since the algorithms themselves performed very well when validated against model “truth” fields. However, these differences are less important given that the system provides a valuable opportunity to comprehensively test algorithms in what has been shown to be a realistic environment.

Making these data more widely available for ground system testing and to users within AWIPS II will be a priority as the launch of GOES-R approaches. We are working with CIRA and NASA’s Short-term Prediction Research and Transition Center (SPoRT) on ways to display and automatically ingest simulated ABI RGB airmass and true-color imagery within AWIPS II for supporting PG testbed activities. Other efforts include providing simulated full-disk ABI imagery based on full spectral resolution GFS meteorological forecasts combined with RAQMS 1° × 1° global

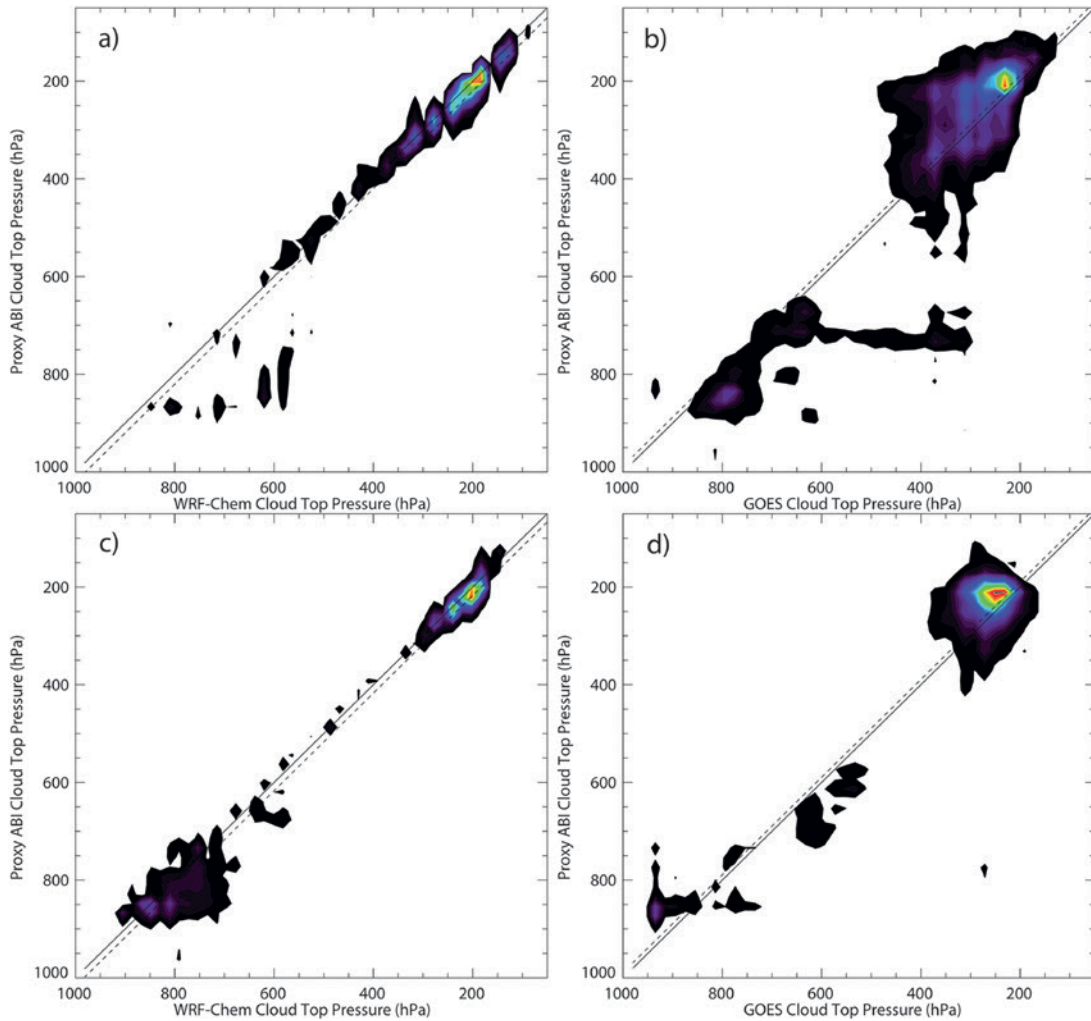


FIG. 11. Density scatterplots of WRF-Chem model and retrieved proxy ABI CTP products for (a) 1200 UTC 26 Oct and (c) 2000 UTC 29 Oct 2012 and retrieved proxy ABI and GOES-13 sounder CTP products for (b) 1200 UTC 26 Oct and (d) 2000 UTC 29 Oct 2012. WRF-Chem model CTPs are defined assuming a total cloud optical depth threshold of 0.1. Dashed lines are mean differences between the datasets.

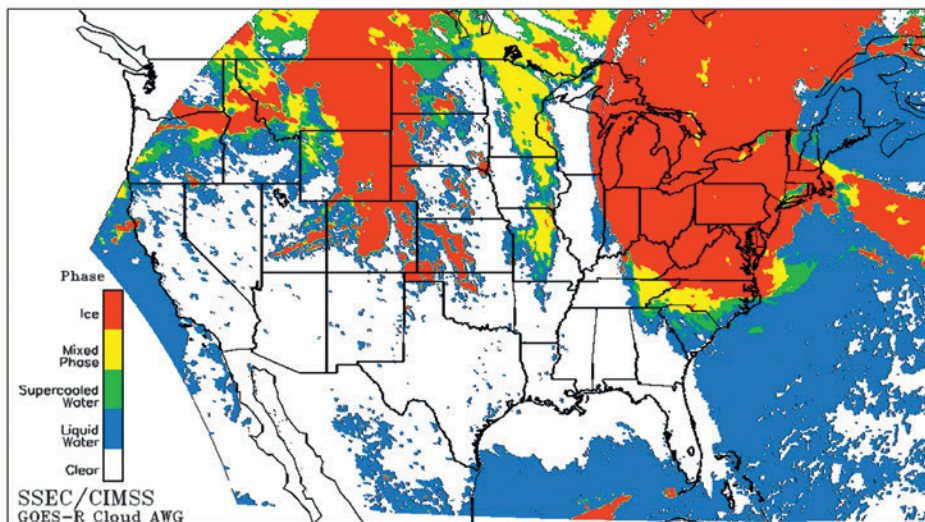


FIG. 12. GOES-13 imager observations of the cloud thermodynamic phase at 2000 UTC 29 Oct 2012.

aerosol predictions to the GOES-R Data Operations Support Team (DOST) for ground system validation.

ACKNOWLEDGMENTS. Support was provided by the GOES-R program through NOAA Cooperative Agreement NA10NES4400013. We wish to thank Graeme Martin for his programming efforts and Brent Holben at NASA for providing the DISCOVER-AQ DRAGON data. We also acknowledge NOAA/NESDIS for providing time on the S4 supercomputer to run the WRF-Chem model and CRTM as part of our real-time system. Special thanks are given to the National Science Foundation–supported TeraGrid and Extreme Science and Engineering Discovery Environment (XSEDE) supercomputing networks for providing computing resources (under Grants OCI-1053575 and ATM060029) to perform high-resolution model simulations during the early years of the project. We also recognize three anonymous reviewers whose comments helped to improve the manuscript. The views, opinions, and findings contained in this report are those of the authors and should not be construed as an official National Oceanic and Atmospheric Administration or U.S. government position, policy, or decision.

REFERENCES

- Bikos, D., and Coauthors, 2012: Synthetic satellite imagery for real-time high-resolution model evaluation. *Wea. Forecasting*, **27**, 784–795, doi:10.1175/WAF-D-11-00130.1.
- Chin, M., R. B. Rood, S.-J. Lin, J. F. Muller, and A. M. Thompson, 2000: Atmospheric sulfur cycle in the global model GOCART: Model description and global properties. *J. Geophys. Res.*, **105**, 24 671–24 687, doi:10.1029/2000JD900384.
- , and Coauthors, 2002: Tropospheric aerosol optical thickness from the GOCART model and comparisons with satellite and sun photometer measurements. *J. Atmos. Sci.*, **59**, 461–483, doi:10.1175/1520-0469(2002)059<0461:TAOTFT>2.0.CO;2.
- Cintineo, R., J. A. Otkin, F. Kong, and M. Xue, 2014: Evaluating the accuracy of planetary boundary layer and cloud microphysical parameterization schemes in a convection-permitting ensemble using synthetic GOES-13 satellite observations. *Mon. Wea. Rev.*, **142**, 163–182, doi:10.1175/MWR-D-13-00143.1.
- Dudhia, J., 1989: Numerical study of convection observed during the Winter Monsoon Experiment using a mesoscale two-dimensional model. *J. Atmos. Sci.*, **46**, 3077–3107, doi:10.1175/1520-0469(1989)046<3077:NSOCOD>2.0.CO;2.
- Dupont, R., and Coauthors, 2012: Attribution and evolution of ozone from Asian wild fires using satellite and aircraft measurements during the ARCTAS campaign. *Atmos. Chem. Phys.*, **12**, 169–188, doi:10.5194/acp-12-169-2012.
- Goodman, S. J., and Coauthors, 2012: The GOES-R Proving Ground: Accelerating user readiness for the next-generation geostationary environmental satellite system. *Bull. Amer. Meteor. Soc.*, **93**, 1029–1040, doi:10.1175/BAMS-D-11-00175.1.
- Grell, G. A., S. E. Peckham, R. Schmitz, S. A. McKeen, G. Frost, W. C. Skamarock, and B. Eder, 2005: Fully coupled online chemistry within the WRF model. *Atmos. Environ.*, **39**, 6957–6975, doi:10.1016/j.atmosenv.2005.04.027.
- Horne, R., 2014: Product definition and users' guide (PUG). Volume 4: GOES-R rebroadcast (GRB). Harris Corporation, Melbourne, FL, 145 pp. [Available online at www.goes-r.gov/users/docs/PUG-GRB-vol4-verC.pdf.]
- Janjić, Z. I., 1994: The step-mountain eta coordinate model: Further developments of the convection, viscous layer, and turbulence closure schemes. *Mon. Wea. Rev.*, **122**, 927–945, doi:10.1175/1520-0493(1994)122<0927:TSMECM>2.0.CO;2.
- Koltunov, A., S. L. Ustin, and E. M. Prins, 2012: On timeliness and accuracy of wildfire detection by the GOES WF-ABBA algorithm over California during the 2006 fire season. *Remote Sens. Environ.*, **127**, 194–209, doi:10.1016/j.rse.2012.09.001.
- Lee, Y.-K., J. A. Otkin, and T. J. Greenwald, 2014: Evaluating the accuracy of a high-resolution model simulation through comparison with MODIS observations. *J. Appl. Meteor. Climatol.*, **53**, 1046–1058, doi:10.1175/JAMC-D-13-0140.1.
- Martin, G., 2007: GEOCAT manual: GEOCAT version 0.5. Cooperative Institute for Meteorological Satellite Studies, University of Wisconsin–Madison, 30 pp. [Available online at ftp://ftp.ssec.wisc.edu/pub/geocat/old/version_0_5/geocat_manual_v0_5.pdf.]
- McMillan, W. W., and Coauthors, 2010: An observational and modeling strategy to investigate the impact of remote sources on local air quality: A Houston, Texas, case study from the Second Texas Air Quality Study (TexAQS II). *J. Geophys. Res.*, **115**, D01301, doi:10.1029/2009JD011973.
- Miller, S. D., C. C. Schmidt, T. J. Schmit, and D. W. Hillger, 2012: A case for natural colour imagery from geostationary satellites, and an approximation for the GOES-R ABI. *Int. J. Remote Sens.*, **33**, 3999–4028, doi:10.1080/01431161.2011.637529.
- Mlawer, E. J., S. J. Taubman, P. D. Brown, M. J. Iacono, and S. A. Clough, 1997: Radiative transfer for inhomogeneous atmospheres: RRTM, a validated correlated-k model for the

- longwave. *J. Geophys. Res.*, **102D**, 16,663–16,682, doi:10.1029/97JD00237.
- Natarajan, M., and Coauthors, 2012: Radiative forcing due to enhancements in tropospheric ozone and carbonaceous aerosols caused by Asian fires during spring 2008. *J. Geophys. Res.*, **117**, D06307, doi:10.1029/2011JD016584.
- Otkin, J. A., and T. J. Greenwald, 2008: Comparison of WRF model-simulated and MODIS-derived cloud data. *Mon. Wea. Rev.*, **136**, 1957–1970, doi:10.1175/2007MWR2293.1.
- , D. J. Posselt, E. R. Olson, H.-L. Huang, J. E. Davies, J. Li, and C. S. Velden, 2007: Mesoscale numerical weather prediction models used in support of infrared hyperspectral measurement simulation and product algorithm development. *J. Atmos. Oceanic Technol.*, **24**, 585–601, doi:10.1175/JTECH1994.1.
- , T. J. Greenwald, J. Sieglaff, and H.-L. Huang, 2009: Validation of a large-scale simulated brightness temperature dataset using SEVIRI satellite observations. *J. Appl. Meteor. Climatol.*, **48**, 1613–1626, doi:10.1175/2009JAMC2142.1.
- Pavolonis, M., 2010: GOES-R Advanced Baseline Imager (ABI) algorithm theoretical basis document for cloud type and cloud phase (version 2.0). NOAA/NESDIS/Center for Satellite Applications and Research, College Park, MD, 96 pp. [Available online at www.goes-r.gov/products/ATBDs/baseline/Cloud_CldType_v2.0_no_color.pdf.]
- Pierce, R. B., and Coauthors, 2007: Chemical data assimilation estimates of continental U.S. ozone and nitrogen budgets during the Intercontinental Chemical Transport Experiment–North America. *J. Geophys. Res.*, **112**, D12S21, doi:10.1029/2006JD007722.
- , and Coauthors, 2009: Impacts of background ozone production on Houston and Dallas, Texas, air quality during the Second Texas Air Quality Study field mission. *J. Geophys. Res.*, **114**, D00F09, doi:10.1029/2008JD011337.
- Schmit, T. J., M. M. Gunshor, W. P. Menzel, J. J. Gurka, J. Li, and A. S. Bachmeier, 2005: Introducing the next-generation Advanced Baseline Imager on GOES-R. *Bull. Amer. Meteor. Soc.*, **86**, 1079–1096, doi:10.1175/BAMS-86-8-1079.
- , J. Li, J. Li, W. F. Feltz, J. J. Gurka, M. D. Goldberg, and K. J. Schrab, 2008: The GOES-R Advanced Baseline Imager and the continuation of current sounder products. *J. Appl. Meteor. Climatol.*, **47**, 2696–2711, doi:10.1175/2008JAMC1858.1.
- Seemann, S. W., E. E. Borbas, R. O. Knuteson, G. R. Stephenson, and H.-L. Huang, 2008: Development of a global infrared land surface emissivity database for application to clear sky sounding retrievals from multispectral satellite radiance measurements. *J. Appl. Meteor. Climatol.*, **47**, 108–123, doi:10.1175/2007JAMC1590.1.
- Shuai, Y., and Coauthors, 2013: Daily MODIS 500 m reflectance anisotropy direct broadcast (DB) products for monitoring vegetation phenology dynamics. *Int. J. Remote Sens.*, **34**, 5997–6016, doi:10.1080/01431161.2013.803169.
- Smith, W. L., Jr., P. Minnis, C. Fleegeer, D. Spangenberg, R. Palikonda, and L. Nguyen, 2012: Determining the flight icing threat to aircraft with single-layer cloud parameters derived from operational satellite data. *J. Appl. Meteor. Climatol.*, **51**, 1794–1810, doi:10.1175/JAMC-D-12-057.1.
- Thompson, G., P. R. Field, R. M. Rasmussen, and W. D. Hall, 2008: Explicit forecasts of winter precipitation using an improved bulk microphysics scheme. Part II: Implementation of a new snow parameterization. *Mon. Wea. Rev.*, **136**, 5095–5115, doi:10.1175/2008MWR2387.1.
- Verma, S., and Coauthors, 2009: Ozone production in boreal fire smoke plumes using observations from the Tropospheric Emission Spectrometer and the Ozone Monitoring Instrument. *J. Geophys. Res.*, **114**, D02303, doi:10.1029/2008JD010108.
- Weisz, E., J. Li, W. P. Menzel, A. K. Heidinger, B. H. Kahn, and C.-Y. Liu, 2007: Comparison of AIRS, MODIS, CloudSat and CALIPSO cloud top height retrievals. *Geophys. Res. Lett.*, **34**, L17811, doi:10.1029/2007GL030676.
- Xie, H., and Coauthors 2013: Integration and ocean-based prelaunch validation of GOES-R Advanced Baseline Imager legacy atmospheric products. *J. Atmos. Oceanic Technol.*, **30**, 1743–1756, doi:10.1175/JTECH-D-12-00120.1.

THE LIFE CYCLES OF EXTRATROPICAL CYCLONES



Edited by Melvyn A. Shapiro and Sigbjørn Grønås

Containing expanded versions of the invited papers presented at the International Symposium on the Life Cycles of Extratropical Cyclones, held in Bergen, Norway, 27 June–1 July 1994, this monograph will be of interest to historians of meteorology, researchers, and forecasters. The symposium coincided with the 75th anniversary of the introduction of Jack Bjerknes's frontal-cyclone model presented in his seminal article, "On the Structure of Moving Cyclones." The monograph's content ranges from a historical overview of extratropical cyclone research and forecasting from the early eighteenth century into the mid-twentieth century, to a presentations and reviews of contemporary research on the theory, observations, analysis, diagnosis, and prediction of extratropical cyclones. The material is appropriate for teaching courses in advanced undergraduate and graduate meteorology.

The Life Cycles of Extratropical Cyclones is available for \$75 list/\$55 members.

To order, visit www.ametsoc.org/amsbookstore, or see the order form at the back of this issue.